Band alignment at the SiO_{2}/HfO_{2} interface: Group IIIA versus group IIIB metal dopants

Xuhui Luo, Gennadi Bersuker, and Alexander A. Demkov

Phys. Rev. B **84**, 195309 — Published 7 November 2011

DOI: 10.1103/PhysRevB.84.195309

Band alignment at the SiO_2/HfO_2 interface: group IIIA vs. group IIIB metal dopants

Xuhui Luo[a], Gennady Bersuker[b] and Alexander A. Demkov[a1]

[a]Department of Physics, The University of Texas at Austin, Austin, Texas 78712, USA

[b]SEMATECH, 2706 Montopolis Dr., Austin, Texas 78741, USA

Abstract:

Using density functional theory we examine the effect of Al and La incorporation on the electronic properties of the interface in the SiO_2/HfO_2 high-k gate stacks recently introduced into the advanced modern field effect transistors. We show that La and Al doping have opposite effects on the band alignment at the SiO_2/HfO_2 interface: while the Al ions, which substitute preferentially for Si in the SiO_2 layer, promote higher effective work function (EWF) values, the substitution of La for Hf decreases EWF. The analysis of the electronic structure of the doped interface suggests a simple relation between the electronegativity of the doping metal, screening properties of the interfacial layer and the band offset, which allows predicting qualitatively the effect of the high-k gate stack doping with a variety of metals on its EWF.

[1] E-mail: demkov@physics.utexas.edu

Introduction

Owing to its large dielectric constant of >20 (the so-called high-k), hafnia (hafnium dioxide HfO_2) and hafnia-based materials are currently used as the gate dielectrics in the advanced complementary metal oxide semiconductor (CMOS) device technology replacing the traditional SiO_2–based dielectrics [1]. This departure from the oxide naturally grown on silicon resulted in multiple challenges in the fabrication process, since the notable inertness of dioxides of metals belonging to the third transition series is achieved only upon heating to temperatures (2500°C) inaccessible in Si technology. One of the challenges for the integration of hafnia in the Si devices is the stringent requirement to keep the operating gate voltage sufficiently low [2, 3]. In order to operate at a bias of about |1| Volt, the transistor threshold voltage has to be less than |200| meV. For that, one needs to use two different gate metals with the work functions closely matching the Si conduction and valence band edges for the n- and p- type transistors, respectively. This turned out to be difficult to achieve in practice. In particular, many high (and to a certain degree low) work function (more than 5 eV) metals, which can be employed to match the valence (conduction) band of Si (the so-called p-type metals) exhibit inherent thermodynamic instability in contact with hafnia when processed under high temperature (>800°C) conditions [4, 5] as required under the gate-first integration scheme.

An alternative way to control the band alignment (and the threshold voltage) would be to develop a gate stack where one can effectively modify the position of the Fermi level of the metal [6, 7]. Experimental attempts of adjusting the Fermi level include doping the gate dielectrics stack, which includes an HfO_2 –based film and a thin layer of SiO_2 (which either spontaneously forms at the interface with the Si substrate or is intentionally grown), with metal ions. In particular, group III metals have been suggested to modify the interfacial dipole. For example, La has been used for the n-type silicon field effect transistors (FETs) [6, 8-11] and Al for the p-type FETs [7, 12-17]. The doping can be achieved, for instance, *via* the ion diffusion from a thin metal oxide capping layer deposited on top of the HfO_2-based dielectric. Recent experimental results for the flat band voltage shift (directly related to the band alignment) tuning by La and Al doping are summarized in Table I. Note that while both metals introduce holes if doped substitutionally, the effect on the band alignment is precisely the opposite. To control the

alignment process we need the microscopic understanding of the role of metal ions in the effective work function modulation at the interface.

Recently, the atomic structure of and band alignment at the un-doped and doped SiO_2/HfO_2 interfaces have been studied theoretically by several groups using density functional theory (DFT) [18-21]. Sharia *et al.* considered the un-doped [18] and Al-doped [19] SiO_2/HfO_2 gate stacks. For the un-doped case, the two lowest energy interface atomic configurations based on the coordination number of oxygen at the interface were identified. For the Al-doped stack, it was found that Al prefers to substitute for Si rather than Hf, and that Al doping lowers the valence band offset. Robertson *et al.* [20, 21] considered substitutional doping of the SiO_2/HfO_2 interfaces with Al, La, Sr and Nb, and demonstrated the shifts of the flat band voltage in the experimentally observed directions, *i.e.* negative for La and Sr and positive for Al and Nb; however, no calculations of the interstitial doping at the SiO_2/HfO_2 have been reported.

The most important aspect of the SiO_2/HfO_2 interface in the context of the effective work function is the microscopic picture of the band alignment. It was argued [18] that the dipole correction to the Schottky limit at the SiO_2/HfO_2 interface can be split in two contributions: charge "spreading" across the interface and screening of this charge by polarizable oxygen ions. It was determined that the screening ability of oxygen at the interface is controlled by the oxygen coordination that allowed introducing a simple model predicting the valence band offset (VBO), in good agreement with first principles calculations and experimental results. More recently, Cockayne has investigated theoretically the effect of an oxygen vacancy on the dielectric properties of bulk hafnia and shown that depending on the vacancy charge state, it may enhance or reduce the dielectric constant [22]. He found that the presence of neutral vacancies in the concentration range of 1.6% increases the dielectric constant by approximately 2% due to higher polarizability of the F-center; while in the 2+ charge state the vacancies decreases the dielectric constant by the same amount due to the phonon hardeninig. Though later effect was neglected in [18], the overall vacancy effect is small.

Similarly, the doping effect on the band alignment has been discussed in terms of bond dipoles [23], oxygen vacancies [6], and electronegativity [24]. Sharia reported that substitution of Si with Al at the interface results in a smaller VBO [19]. They attribute the effect to the reduction of the interface screening to increasing density of oxygen vacancies caused by the Al^{3+} substitution for the Si^{4+}. This argument leaves open the question why doping with La, also a

trivalent metal, increases the VBO. Recently, Lin and Robertson *et al.* [20] applied the image charge model to the SiO_2/HfO_2 interface making the electrostatic arguments in an attempt to explain the effect of La doping. However, the applicability of this approach is not clear since the screening mechanism in the high k-materials is different from that in the metals.

In this paper, we report a systematic study of the Al and La doped SiO_2/HfO_2 interfaces using first principles calculations. First, we provide the detailed analyses of the atomic structure of the un-doped and doped interface. We then discuss the electronic structure of the interface including the mechanism of charge transfer and band alignment. We propose a simple physical model describing the band alignment of doped interfaces.

Computational and modeling details

Density functional theory (DFT) calculations within the general gradient approximation (GGA) are carried out using the Vienna *ab* initio Simulation Package (VASP) [25]. We employ the generalized gradient approximation (GGA) [26] and projection augmented wave (PAW) pseudopotentials [27]. For Hf and La atoms 5d and 6s electrons are included, while 2s and 2p electrons are included for oxygen. We include 3s and 3p electrons for Si and Al. The Brillouin zone integration is performed using a 8×8×8 Monkhorst-Pack [28] special k-point grid for bulk SiO_2 and HfO_2. The kinetic energy cutoff of 600 eV is found to ensure the total energy convergence to 10^{-6} eV/atom. The full structural relaxation is performed until the Hellmann-Feynman forces are less than 0.02 eV/Å.

To simulate the interface we employ slab geometry. We use structural models of the SiO_2/HfO_2 interface introduced in Ref [18], where monoclinic HfO_2 was connected to β-cristobalite SiO_2. Following the nomenclature of Ref. [18] our starting models are called m332 and m322 as shown in Fig. 1a and Fig. 1b. The number refers to the coordination number of three bridge oxygen atoms. For example, the m332 interface has two three-fold bridge oxygen atoms and one two-fold oxygen atom at the interface ('m" indicates that monoclinic hafnia is used). Note that the total energy of m332 is 0.94 eV/cell less than that of m322 [18]. A 15 Å thick vacuum layer is added in the direction normal to the interface to eliminate spurious slab-slab interactions. We use the conjugate-gradient algorithm to optimize the atomic structure for both undoped and doped interfaces. Because the lateral dimensions of the simulation cell is the

same as those of the $\sqrt{2}\times\sqrt{2}$ (001) cell of β-cristobalite SiO_2 surface, the k-point mesh is chosen to be 4×4×1 to make sure that the bulk and slab calculations have the same precision.

Atomic structure of the interface

When considering the doping of an interface the following basic questions need to be answered: 1) whether the dopant indeed segregates to the interface or prefers staying in the bulk on either side of the interface; 2) which side of the interface is energetically preferred, and 3) whether the dopant goes in substitutionally or interstitially. In order to gain a better understanding of the interaction between the two oxides and trivalent metals, we start by considering the interstitial doping of Al and La in the bulk SiO_2. It has been shown [19] that Al prefers to substitute for Si at the interface, so here we focus on La doping. We find that inserting large La atoms interstitially into HfO_2 is not energetically favorable, which is not surprising since hafnia has much less open structure than bulk SiO_2 (Table II). Furthermore, we find that stoichiometric interstitial doping of La in bulk SiO_2 (one oxygen vacancy is introduced for every two La atoms) is also less stable than substitutional doping. We infer the following picture for the La doping in SiO_2. In the low concentration limit, La atoms choose to substitute Si, and the stoichiometric requirement on oxygen causes the breaking of the tetrahedral network. As the concentration of La increases, the network breaks into the isolated SiO_4 tetrahedra, and lanthanum silicate forms. Therefore, we don't consider interstitial doping in the following discussion.

As for the doping of the interface itself, we start by comparing the doping effects between m332 and m322 interfaces and then focus on the doped m332 structures. We substitute the original metal M (M could be Si and Hf) at the interface by the doping metal D (D could be Al or La). The resulting doped structure is labeled as D_M. Thus we have four combinations for each interface: La_{Si}, La_{Hf}, Al_{Si} and Al_{Hf}. We try several possible structures for each combination. The structure with the lowest energy is chosen as the representative one. Figs. 2 a-d show the un-relaxed and relaxed m332 structures doped with La. Fig. 2a and 2c are the structures of La_{Si} and La_{Hf} before relaxation. Fig. 2b and 2d are the corresponding relaxed structures. The coordination number of the La atoms and La-O bond lengths before and after relaxation are listed in Table III. Before relaxation the coordination number of La by oxygen is four for the structure La_{Si}, which is the same as the coordination number of Si in the SiO_2. In the relaxed La_{Si} structure one of the

doped La atoms keeps the four-fold coordination and the other La atom changes to being five-fold. In the un-relaxed La_{Hf} structure one La has the coordination number of seven and the other La is five-fold. After relaxation the initially five-fold coordinated La atom becomes six-fold coordinated and the seven-fold La is unchanged. This suggests that La atoms try to increase the coordination number after substitution. We also compare the bond lengths of La-O before and after relaxation and find La-O bond lengths increase upon relaxation. In all La doped interfaces the coordination number of doping atoms increases after relaxation and so does the La-O bond length. On the other hand, Al doping shows quite different behavior (see Fig. 3a-3d). The Al-O bond length increases from 1.63 Å to 1.89 Å for Al_{Si} and decreases from 2.20 Å to 1.92 Å for Al_{Hf} after relaxation. The coordination number of Al has the same trend as the Al-O bond length during relaxation. The relaxed Al-O bond length for Al_{Si} is similar to that in aluminum silicates [32].

To find out whether the dopant prefers to substitute Si or Hf at the SiO_2/HfO_2 interface we need to compare the energies of different substitutions. Since the numbers of Si and Hf atoms are different, the direct comparison of the total energy is not possible. Suppose an undoped m332 structure has *m* SiO_2 and *n* HfO_2 formula units, then the D_{Si} structure contains (*m-2*) SiO_2, *n* HfO_2 and one D_2O_3. Similarly, a D_{Hf} structure contains *m* SiO_2, (*n-2*) HfO_2 and one D_2O_3. One way to circumvent this difficulty would be to introduce chemical potentials and consider the Gibbs free energy in various reactions. Here we use a somewhat simpler approach: we consider the substitution via two reactions:

$m332+La_2O_3 \rightarrow D_{Si}+2SiO_2$

$m332+La_2O_3 \rightarrow D_{Hf}+2HfO_2$

This amounts to dividing a doped structure into five regions as shown in Fig. 4a: SiO_2 surface, SiO_2 bulk, interface region, HfO_2 bulk and HfO_2 surface. If we insert two more SiO_2 molecules in the SiO_2 bulk region of the D_{Si} structure (Fig. 4b) and two HfO_2 molecules in the HfO_2 bulk region of the D_{Hf} structure (Fig. 4c), we don't change the physics at the interface or surface. At the same time, modified D_{Si} and D_{Hf} now have the same composition. The two new structures are called D_{Si}' and D_{Hf}', and we have:

$$E_{D_{Si}'} = E_{D_{Si}} + 2E_{bulk\_SiO_2}$$
$$E_{D_{Hf}'} = E_{D_{Hf}} + 2E_{bulk\_HfO_2}$$

Since now the numbers of the MO_2 units in the bulk region are the same for D_{Si}' and D_{Hf}', the energy difference between D_{Si}' and D_{Hf}' is equal to that of the interface region between D_{Si} and D_{Hf}. Comparing the energy of D_{Si}' and D_{Hf}' we can identify the energetically preferred substitution. The calculated energy differences $\Delta E = E_{D_{Si}'} - E_{D_{Hf}'}$ are listed in Table IV. Our results strongly suggest that in the case of La doping, La would segregate on the Hf sites (La_{Hf} structure is preferred energetically). On the other hand, in the case of Al doping, Al prefers substituting for Si.

However, even with the estimates presented in Table IV, assigning the dopant to a particular side of the interface is not always straightforward. After relaxation the La and oxygen atoms at the interface reconstruct and their coordination numbers change slightly. As a result, the relaxed doped interface doesn't have a clear boundary between the SiO_2 and HfO_2 sides. We use the coordination number of metal atoms and the length of metal-oxygen bonds to assign the dopant location. In Table V we list the average coordination numbers, average metal-oxygen bond lengths, and metal electronegativity in the crystalline SiO_2, HfO_2, Al_2O_3 and La_2O_3. As can be seen in table III, after relaxation the coordination number and metal-oxygen bond lengths tend to become closer to the corresponding bulk values. For example, in the Al_{Si} structure, Al clearly assumes the coordination number and Al-O bond length similar to those in bulk Al_2O_3. Following this observation, we qualitatively assign the preferential dopant location. La prefers the ionic, highly coordinated environment while Al prefers the covalent environment and strong bonding with oxygen. Since HfO_2 is an ionic compound with highly coordinated metal, then La prefers staying on the HfO_2 side. On the other hand, SiO_2 is a largely covalent tetrahedral framework, and Al prefers to substitute for Si. This, as will be shown below, has the profound effect on the band alignment at the interface.

Band alignment and charge transfer

We use the reference potential method originally introduced by Kleinman *et al.*[33-35] to calculate the valence band offset (VBO). The macroscopically averaged electrostatic potential is used as reference energy [34]. In the supercell, we first average the electrostatic potential over the x-y plane to get the planar average potential and then average it along the z axis to obtain the smooth macroscopic potential:

$$\overline{V}(z) = \frac{1}{d_1 d_2} \int_{z-d_1/2}^{z+d_1/2} dz' \int_{z'-d_2/2}^{z'+d_2/2} dz'' \iint dx dy \, V(x, y, z'')$$

where d_1 and d_2 are the periodic cell dimensions in bulk regions of SiO_2 and HfO_2 along the z direction. This method requires two additional bulk calculations of SiO_2 and HfO_2 to place the energy of the valence band top (VBT) with respect to the average potential in the bulk. The difference in the VBT of SiO_2 and HfO_2 is the calculated valence band offset. Figure 5 shows the planar and macroscopically averaged potential of the m332 undoped structure as an example of calculating the VBO. Table VI lists VBOs for all considered doping combinations of m332 and m322 interfaces. Our calculations suggest that Al doping will decrease the VBO and may even change the relative position of two valence band edges while La doping will increase the VBO regardless whether we dope at the SiO_2 or HfO_2 side of the interface.

The second derivative of the macroscopic average potential is related to the macroscopic charge density *via* the Poisson equation:

$$\nabla^2 \overline{V} = -\frac{\rho}{\varepsilon}$$

here ε is the local dielectric constant. This allows for a qualitative discussion of the so-called interface dipole. In Figure 6 we show ρ/ε at the m332 interface doped with Al and La. We also show the un-doped case as a reference. As expected for the interfacial double layer, ρ/ε at the un-doped interface has negative and positive charge regions in the SiO_2 and HfO_2, respectively. We find that the Al-doped interface (Al_{Si}) has a ρ/ε profile similar to that of the un-doped interface (see Fig. 6a). However, the La doped interface (La_{Hf}) has a totally different ρ/ε profile consisting of three distinct regions: the negative, positive and negative again (see Fig. 6b). To see the bare charge distribution without the ε factor, we directly calculate the charge density at the interface. Of course, the pseudopotential DFT method includes only the valence electrons:

$$\rho_{valence}(x,y,z) = \sum_{\substack{occupied \\ states\ i}} |\varphi_i(x,y,z)|^2$$

where φ_i is the occupied eigen states of the Kohn-Sham equation. The core charges are composed of the electrons in the core states and bare ionic charges:

$$\rho_{core}(x,y,z) = \rho_{core\,electrons}(x,y,z) + \rho_{ion}(x,y,z).$$

The core charges are assumed to be located at the atomic positions and their distribution is described by the Dirac delta function. In a neutral solid, the sum of the valence and core charges globally adds to zero. For the interface structures, we use the macroscopic averaging procedure to smooth the total charge density:

$$\overline{\rho}_{total}(z) = \frac{1}{d_1 d_2}\int_{z-d_1/2}^{z+d_1/2} dz' \int_{z'-d_2/2}^{z'+d_2/2} dz'' \iint dxdy\,[\rho_{valence}(x,y,z'') + \rho_{core}(x,y,z'')]$$

Figures 7a and 7b show the averaged total charge density (including both valence and core charges), for the Al-doped (Al_{Si}) and La-doped (La_{Hf}) interfaces, respectively. The important difference between two metals is that in the case of La the presence of a second double layer with the opposite dipole.

Overall, our results summarized in table VI are in a qualitative agreement with the recent experiments [6-17], and we need to identify the microscopic mechanism of the doping effect. Sharia *et al.* have discussed the band alignment problem for the undoped SiO_2/HfO_2 interface; it was suggested that the charge transfer from HfO_2 to SiO_2 due to the electronegativity difference is screened by the oxygen polarization at the interface [18]. The VBO was estimated taking the dipole correction to the Schottky's limit of the band offset:

$$VBO_0 = V_{Schottky} - \frac{\rho d^2}{2\varepsilon_0 \varepsilon_{ox}},$$

where ρ is the density of transferred charge, $2d$ is the thickness of the double layer and ε_{ox} is the effective dielectric constant of the interface. It was further assumed that the dielectric constant ε_{ox} varied with the coordination number of the interfacial oxygen atoms. In the case of a doped interface, several additional factors play a role in the band alignment complicating this picture. Qualitatively, we assign the dopant to either SiO_2 or HfO_2 side according to its coordination

number and bond lengths with oxygen. Then, in addition to the charge transfer between two oxides discussed by Sharia (we shall call it the oxide charge transfer q_{ox}), a charge transfer between the dopant and its surrounding occurs. We shall call it the internal charge transfer q_i. As we have shown, the dopant chooses the side of the interface where the metal has similar chemical properties. Thus we expect q_i to be smaller than q_{ox}. Conceptually, we can think of two capacitors connected in series. We further assume the oxide charge transfer q_{ox} and the interfacial dielectric constant are the same for all interfaces. These two assumptions help us to capture the essential physics in a simple picture. Later we shall discuss the effect of the dielectric constant variation.

First we discuss the oxide charge transfer and internal charge change in terms of electronegativity. Without doping, the double layer of the dipole in the interface region results in a relatively abrupt change of the average electrostatic potential. As seen from Figures 6b and 7b, La atoms at the interface lead to a large change of the interface dipole, while Al atoms cause only a minor redistribution. This can be understood as caused by the difference in metal electronegativity [36]. The Pauli electronegativity decreases from Si to Al, to Hf, and to La (see Table V). At the un-doped SiO_2/HfO_2 interface, HfO_2 transfers q_{ox} electrons to SiO_2 because of the electronegativity difference as seen in Fig. 8a. When Al is introduced in the region between SiO_2 and HfO_2 as shown in Fig. 8b, Hf transfers electrons to Al, while Al transfers electrons to Si (the electronegativity of Al is between those of Si and Hf), and the resulting internal charge transfer q_i is qualitatively the same as the oxide charge transfer. Therefore, Al doping has a mild effect on the interface dipole. Overall, the amount of transferred charge in Al-doped interface increases by approximately 5% as shown in the Figs. 6a and 7a. On the other hand, the electronegativity of La is less than that of either Si or Hf, and therefore La loses electrons to both of them. In this case, q_{ox} and q_i exhibit opposite signs and the resulting magnitude of the dipole is greatly affected by the La doping as seen in Fig. 6b and 7b.

This can be described in a generalized capacitor model similar to that proposed by Sharia [18]. As we have shown, Al prefers to stay at the SiO_2 side of the interface. Therefore, the internal capacitor is considered to be located at the SiO_2 side (Figure 8b), and the VBO could be written as:

$$VBO_{Al} = V_{Schottky} - \frac{\rho_o d_0^{\,2}}{2\varepsilon_0\varepsilon_{ox}} - \frac{\rho_{i1} d_1^{\,2}}{2\varepsilon_0\varepsilon_{i1}},$$

where ρ_{i1} is the density of the internal transferred charge from Al to Si and $2d_1$ is the distance between two dipole layers induced by the internal charge transfer. The additional internal capacitor increases the potential difference ΔU_{Al} and hence decreases the VBO magnitude.

Being the least electronegative of both Hf and Si, La when inserted between the SiO_2 and HfO_2, is expected to donate electrons to both SiO_2 and HfO_2. Although the electronegativity difference between La and Si is significantly larger than that between La and Hf, charge flows mostly to Hf because of a geometric proximity (see Fig. 8b). Within the Sharia's description, the interface charge transfer decreases, and the VBO value moves back to the Schottky limit:

$$VBO_{La} = V_{Schottky} - \frac{\rho_o d_0^{\,2}}{2\varepsilon_0\varepsilon_{ox}} + \frac{\rho_{i2} d_2^{\,2}}{2\varepsilon_0\varepsilon_{i2}},$$

where ρ_{i2} is the density of the internal transferred charge and $2d_2$ is the distance between two dipole layers induced by the internal charge transfer. Assuming that the dielectric constant of the oxide capacitor ε_{ox} is the same in both cases, one gets $VBO_{Al} < VBO_0 < VBO_{La}$.

Until now we haven't considered the variation of the dielectric constant between different interfaces. Microscopically the media in the oxide and internal capacitors are the oxygen atoms between different metal cations shown in the Fig. 8. In the spirit of Ref. 19, using the coordination number of oxygen (see Table V), we argue that for the lowest energy m332 Al-doped interface all dielectric constants are approximately the same, while for the lowest energy m332 La-doped interface there is an increase in both the oxide and internal dielectric constants as compared to the un-doped structure. The above analysis suggests that the opposite effects of Al and La doping on the band offset at the SiO_2/HfO_2 interface mainly arise from the electronegativity difference between the dopant and original atoms. This suggests that group IIIA metals would have a larger effect on the band alignment because the electronegativity of group IIIB shows much less variation due to the screening provided first by $3d^{10}$ and then $4f^{14}$ inner shell electrons.

Conclusions

In this paper we discuss the structural and electronic properties of un-doped and doped SiO_2/HfO_2 interfaces. Using first principles calculations we show that at low concentration, both group IIIA and IIIB metal dopants prefer substitutional positions in SiO_2 and HfO_2. We then consider substitutional doping of the SiO_2/HfO_2 interface with La and Al. We find that Al prefers the SiO_2 side of the interface, while the lowest energy configuration for La is to substitute for Hf. Generalizing these results we argue that a metal dopant would prefer residing in the lattice matrix whose chemical environment is closer to that of the oxide formed by this metal. For example, Al_2O_3 is closer to SiO_2 and La_2O_3 is closer to HfO_2. We calculate the charge transfer and valence band offset for several doped interface structures from first principles. The analysis of the electrostatic potential and charge distribution suggests that La doping has a significant effect on charge transfer while Al doping has a relatively modest effect. Following a simple capacitor model introduced in [18] for SiO_2/HfO_2 interfaces, we argue that the initial charge distribution (the charge neutrality level alignment) can be altered when a metal less electronegative than Hf is introduced at the hafnia side of the SiO_2/HfO_2 interface pushing the alignment back to its Schottky limit. All structures considered in this study are stoichiometric, and can be viewed as containing compensated oxygen vacancies. The difference in oxygen coordination discussed by Sharia in [19] amplifies the electrostatic effect of doping, but appears to be secondary to changes in the interfacial dipole. This strongly points to group IIIA metals as effective means of controlling the band alignment since they show a larger variance in electronegativity across the group.

Acknowledgements

We thank John Ekerdt and Alexandra Navrotsky for insightful discussions. This work was supported by the National Science Foundation under grant DMR-0606464 and Texas Advanced Computing Center.

Reference

1. 2007 International Technology Roadmap for Semiconductors, Semiconductor Industry Association, San Jose, 2007.
2. S. Sayan, T. Emge, E. Garfunkel, X. Y. Zhao, L. Wielunski, R. A. Bartynski, D. Vanderbilt, J. S. Suehle, S. Suzer and M. Banaszak-Holl, J. Appl. Phys. **96**, 7485 (2004).
3. H. C. Wen, P. Majhi, K. Choi, C. S. Park, H. N. Alshareef, H. R. Harris, H. Luan, H. Niimi, H. B. Park, G. Bersuker, P. S. Lysaght, D. L. Kwong, S. C. Song, B. H. Lee and R. Jammy, Microelectron. Eng. **85**, 2 (2008).
4. A. A. Demkov, Phys. Rev. B **74**, 085310 (2006).
5. G. Bersuker, C. S. Park, H. C. Wen, K. Choi, J. Price, P. Lysaght, H. H. Tseng, O. Sharia, A. Demkov, J. T. Ryan and P. Lenahan, IEEE Trans. Electron Devices **57**, 2047-2056 (2010).
6. S. Guha, V. K. Paruchuri, M. Copel, V. Narayanan, Y. Y. Wang, P. E. Batson, N. A. Bojarczuk, B. Linder and B. Doris, Appl. Phys. Lett. **90**, 092902 (2007).
7. H. N. Alshareef, H. F. Luan, K. Choi, H. R. Harris, H. C. Wen, M. A. Quevedo-Lopez, P. Majhi and B. H. Lee, Appl. Phys. Lett. **88**, 112114 (2006).
8. H. N. Alshareef, M. Quevedo-Lopez, H. C. Wen, R. Harris, P. Kirsch, P. Majhi, B. H. Lee, R. Jammy, D. J. Lichtenwalner, J. S. Jur and A. I. Kingon, Appl. Phys. Lett. **89**, 232103 (2006).
9. C. K. Chiang, C. H. Wu, C. C. Liu, J. F. Lin, C. L. Yang, J. Y. Wu and S. J. Wang, J. Electrochem. Soc. **158**, H447-H451-H447-H451 (2011).
10. W. J. Maeng, W.-H. Kim and H. Kim, J. Appl. Phys. **107**, 074109-074109 (2010).
11. B. J. O'Sullivan, R. Mitsuhashi, G. Pourtois, M. Aoulaiche, M. Houssa, N. Van der Heyden, T. Schram, Y. Harada, G. Groeseneken, P. Absil, S. Biesemans, T. Nakabayashi, A. Ikeda and M. Niwa, J. Appl. Phys. **104**, 044512-044512 (2008).
12. H. J. Li and M. I. Gardner, IEEE Electron Device Lett. **26**, 441 (2005).
13. C. C. Hobbs, L. R. C. Fonseca, A. Knizhnik, V. Dhandapani, S. B. Samavedam, W. J. Taylor, J. M. Grant, L. G. Dip, D. H. Triyoso, R. I. Hegde, D. C. Gilmer, R. Garcia, D. Roan, M. L. Lovejoy, R. S. Rai, E. A. Hebert, H. H. Tseng, S. G. H. Anderson, B. E. White and P. J. Tobin, IEEE Trans. Electron Devices **51**, 971 (2004).
14. W. J. Maeng, W.-H. Kim, J. H. Koo, S. J. Lim, C.-S. Lee, T. Lee and H. Kim, Appl. Phys. Lett. **96**, 082905-082905 (2010).
15. H. N. Alshareef, K. Choi, H. C. Wen, H. Luan, H. Harris, Y. Senzaki, P. Majhi, B. H. Lee, R. Jammy, S. Aguirre-Tostado, B. E. Gnade and R. M. Wallace, Appl. Phys. Lett. **88**, 072108 (2006).
16. K. Xiong, J. Robertson, G. Pourtois, J. Pétry and M. Müller, J. Appl. Phys. **104**, 074501-074501 (2008).
17. N. Yoshida, X. Tang, K. Ahmed, G. Conti, D. Liu, M. Agustin, S. Hung, V. Ku, O. Chan, R. Liang, H. Chen, R. Wang, B. Zheng, C. Lazik, M. Jin, K. Lavu, C.-P. Chang, T. Mandrekar and S. Gandikota, ECS Trans. **13**, 143 (2008).
18. O. Sharia, A. A. Demkov, G. Bersuker and B. H. Lee, Phys. Rev. B **75**, 035306 (2007).
19. O. Sharia, A. A. Demkov, G. Bersuker and B. H. Lee, Phys. Rev. B **77**, 085326 (2008).
20. L. Lin and J. Robertson, Appl. Phys. Lett. **95**, 012906 (2009).
21. L. Lin and J. Robertson, J. Appl. Phys. **109**, 094502 (2011).
22. E. Cockayne, Phys. Rev. B **75**, 094103 (2007).

23. P. D. Kirsch, P. Sivasubramani, J. Huang, C. D. Young, M. A. Quevedo-Lopez, H. C. Wen, H. Alshareef, K. Choi, C. S. Park, K. Freeman, M. M. Hussain, G. Bersuker, H. R. Harris, P. Majhi, R. Choi, P. Lysaght, B. H. Lee, H. H. Tseng, R. Jammy, T. S. Boscke, D. J. Lichtenwalner, J. S. Jur and A. I. Kingon, Appl. Phys. Lett. **92**, 092901 (2008).
24. R. D. Clark, S. Consiglio, C. S. Wajda, G. J. Leusink, T. Sugawara, H. Nakabayashi, H. Jagannathan, L. F. Edge, P. Jamison, V. K. Paruchuri, R. Iijima, M. Takayanagi, B. P. Linder, J. Bruley, M. Copel and V. Narayanan, in *Atomic Layer Deposition Applications 4*, edited by A. Londergan, S. F. Bent, S. DeGendt, J. W. Elam, S. B. Kang and O. VanderStraten (2008), Vol. 16, pp. 291-305.
25. G. Kresse and J. Furthmüller, Phys. Rev. B **54**, 11169 (1996).
26. J. P. Perdew, K. Burke and M. Ernzerhof, Phys. Rev. Lett. **77**, 3865 (1996).
27. G. Kresse and D. Joubert, Phys. Rev. B **59**, 1758 (1999).
28. H. J. Monkhorst and J. D. Pack, Phys. Rev. B **13**, 5188 (1976).
29. S. S. Todd, J. Am. Chem. Soc. **75**, 3035 (1953).
30. R. W. G. Wychoff, *Crystal Structures*. (Wiley, New York, London, 1965).
31. R. T. Downs and D. C. Palmer, Am. Mineral. **79**, 9 (1994).
32. L. Nguyen Ngoc and H. Vo Van, Phys. Scr. **76**, 165 (2007).
33. L. Kleinman, Phys. Rev. B **24**, 7412 (1981).
34. C. G. Van de Walle, Phys. Rev. B **39**, 1871 (1989).
35. D. M. Bylander and L. Kleinman, Phys. Rev. B **36**, 3229 (1987).
36. C. Pauling, *The Nature of the Chemical Bond*, 3rd ed. (Cornell Press, Ithaca, NY, 1960).

Tables:

Table I. The flat band voltage shift extracted from the CV capacitor measurement after La or Al doping (in Ref. 6 both capacitor and transistor measurements are used).

La doping	Al doping
-0.30─-0.40 eV[6]	0.23 eV[7]
-0.40─-0.55 eV[8]	0.15 eV[14]
-0.45 eV[9]	~0.4 eV[15]
-0.35 eV[10]	~0.2 eV[16]
-0.3─-0.5 eV[11]	0.16─0.19 eV[17]

Table II. Calculated and experimental structural parameters for bulk HfO_2 and SiO_2. Experimental data for m-HfO2, and cubic and tetragonal forms of cristobalite are from references 29, 30 and 31, respectively.

	Theory (current work)	Experiment
Monoclinic HfO_2 (4 HfO_2/unit)		
V ($Å^3$)	138.61	138.64
a (Å)	5.1229	5.117
b (Å)	5.1958	5.175
c (Å)	5.2837	5.291
β	99.68°	99.22°
ρ_{Hf} ($Å^{-3}$)	0.0289	
High temperature β-cristobalite SiO_2 (cubic C9 structure with 8 SiO_2)		
V ($Å^3$)	414.05	395.44
a (Å)	7.453	7.34
ρ ($Å^{-3}$)	0.0193	
Low temperature β-cristobalite SiO_2 (tetragonal $I\bar{4}2d$ structure with 4 SiO_2)		
V ($Å^3$)	182.91	172.17
a (Å)	5.079	4.978
b (Å)	7.090	6.948
ρ ($Å^{-3}$)	0.0219	

Table III. The change of coordination number and bond length of dopant during relaxation.

		CN of doping atom I	CN of doping atom II	Bond length of dopant-O (Å)	Trend
Al_{Si}	Unrelaxed	4	3	1.63	↑
	relaxed	5	4	1.89	
Al_{Hf}	Unrelaxed	5	6	2.20	↓
	relaxed	5	5	1.92	
La_{Si}	Unrelaxed	4	4	1.63	↑
	relaxed	4	5	2.40	
La_{Hf}	Unrelaxed	7	5	2.07	↑
	relaxed	7	6	2.52	

Table IV. Energy difference between Si and Hf substitution.

	$\Delta E_{Al} = E_{Al_{Si}'} - E_{Al_{Hf}'}$	$\Delta E_{La} = E_{La_{Si}'} - E_{La_{Hf}'}$
m332	-0.257 eV	0.542 eV
m322	-1.5227 eV	1.541 eV

Table V. Average coordination number (CN), metal-oxide bond length and metal electronegativity in four oxides.

	SiO_2	Al_2O_3	HfO_2	La_2O_3
Average CN of Metal	4	6	7	7
Average CN of Oxygen	2	4	7/2	14/3
The Length of metal-oxygen bonds (Å)	1.67	1.90	2.42	2.74
Electronegativity of Metal	1.90	1.61	1.30	1.10

Table VI. Calculated valence band offsets for m332 and m322 interfaces with and without doping.

VBO (eV)	**Al_{Si}**	**Al_{Hf}**	**No dopant**	**La_{Si}**	**La_{Hf}**
m332	-0.54	0.15	0.56	0.81	0.79
m322	-0.75	-0.70	0.01	0.83	0.87

FIGURE CAPTIONS

Figure 1.

(a) The structure of m332 SiO_2/HfO_2 interface. (b) The structure of m322 SiO_2/HfO_2 interface.

Figure 2.

(a) The un-relaxed m332 structure with La doped in SiO_2 side. (a) The relaxed m332 structure with La doped in SiO_2 side. (c) The un-relaxed m332 structure with La doped in HfO_2 side. (d) The relaxed m332 structure with La doped in HfO_2 side.

Figure 3.

(a) The un-relaxed m332 structure with Al doped in SiO_2 side. (a) The relaxed m332 structure with Al doped in SiO_2 side. (c) The un-relaxed m332 structure with Al doped in HfO_2 side. (d) The relaxed m332 structure with Al doped in HfO_2 side.

Figure 4.

(a) Partition of an un-doped structure. (b) Partition of an interface with La doped in SiO_2 side. (c) Partition of an interface with La doped in HfO_2 side.

Figure 5.

A composite graph of the plane averaged electrostatic potential and its macroscopic average of the un-doped m332 interface.

Figure 6.

(a) Comparison of the second derivative of the macroscopic averaged electrostatic potential of un-doped and Al-doped interfaces. (b) Comparison of the second derivative of the macroscopic averaged electrostatic potential of un-doped and La-doped interfaces.

Figure 7.

(a) Comparison of the macroscopic averaged charge distribution of un-doped and Al-doped interfaces. (b) Comparison of the macroscopic averaged charge distribution of un-doped and La-doped interfaces.

Figure 8.

(a) The schematic graph of charge transfer in the un-doped m332 interface and its corresponding physical model. (b) The schematic graph of charge transfer in the Al-doped m332 interface and

its corresponding physical model. (c) The schematic graph of charge transfer in the La-doped m332 interface and its corresponding physical model.

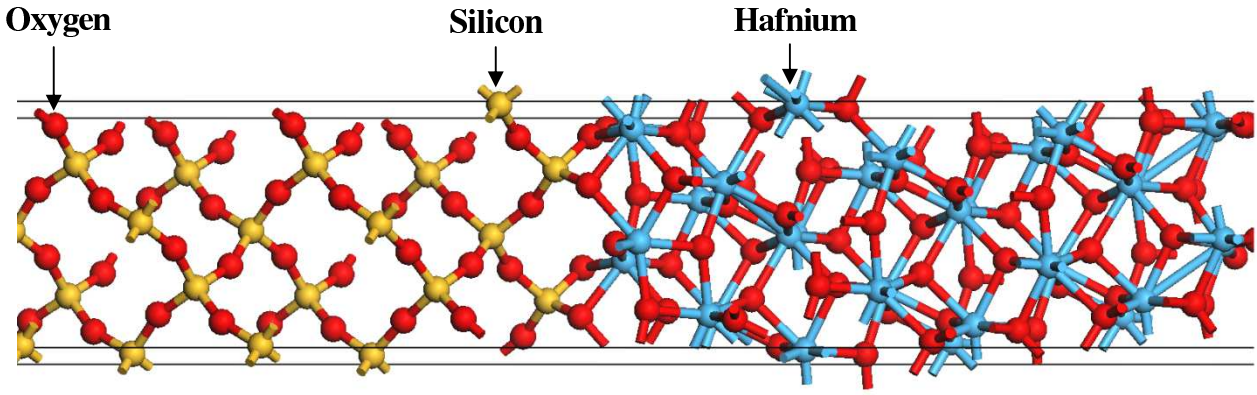

Figure 1a BF11791 27SEP2011

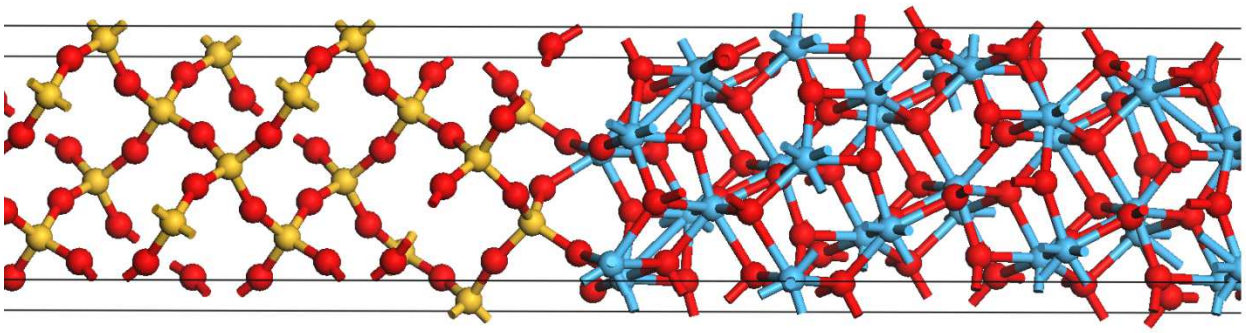

Figure 1b BF11791 27SEP2011

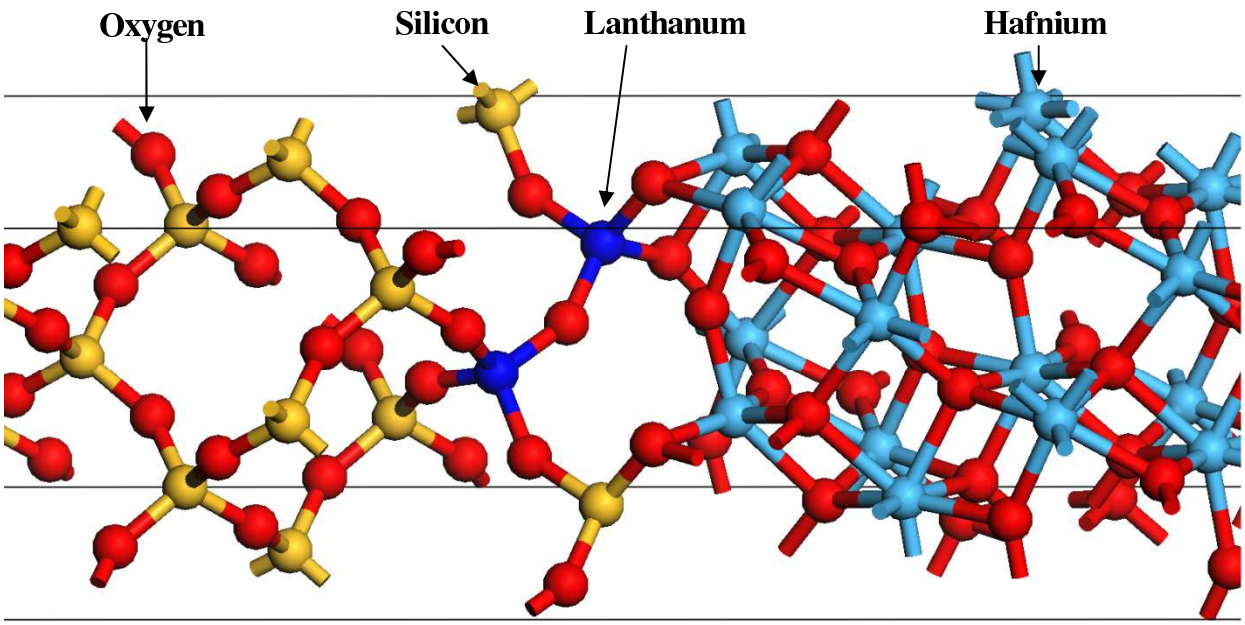

Figure 3a BF11791 27SEP2011

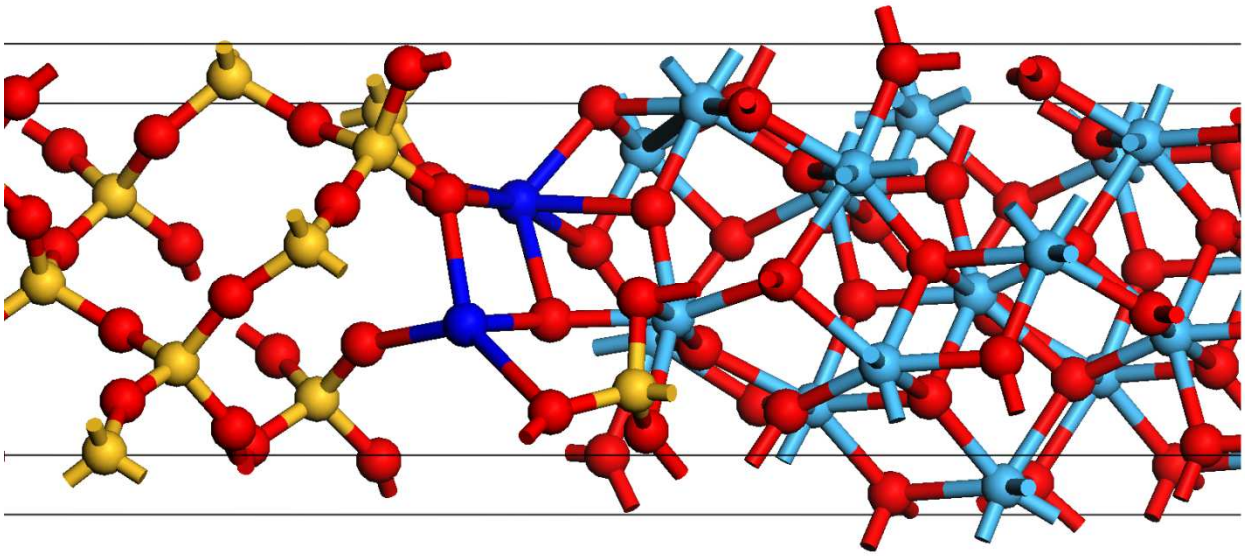

Figure 3b BF11791 27SEP2011

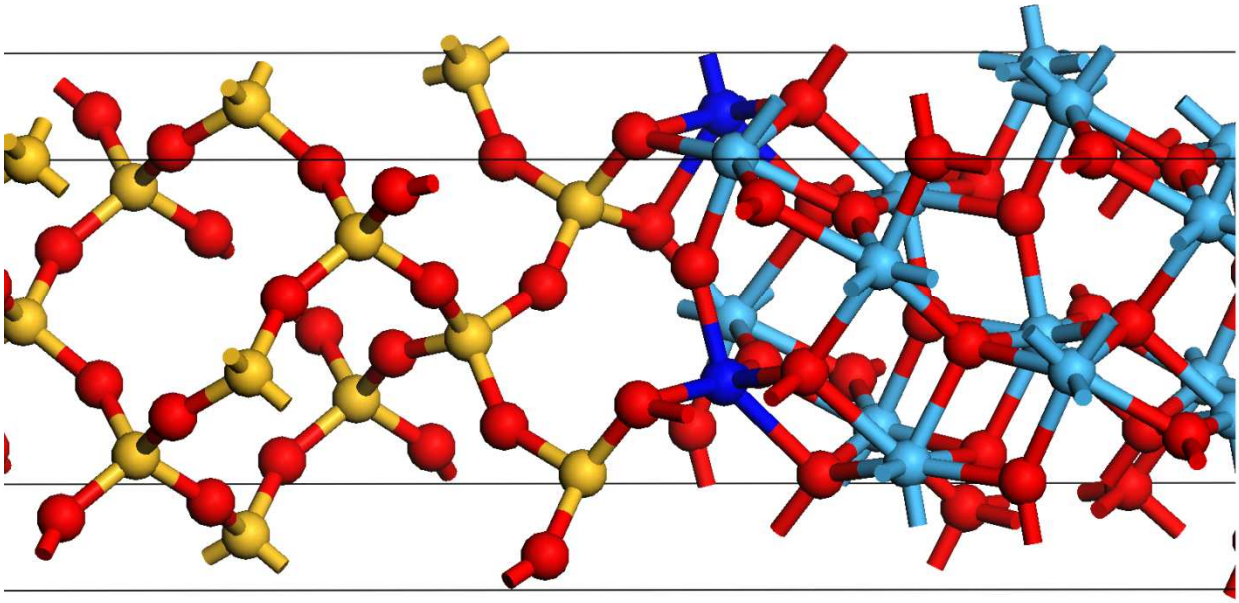

Figure 3c BF11791 27SEP2011

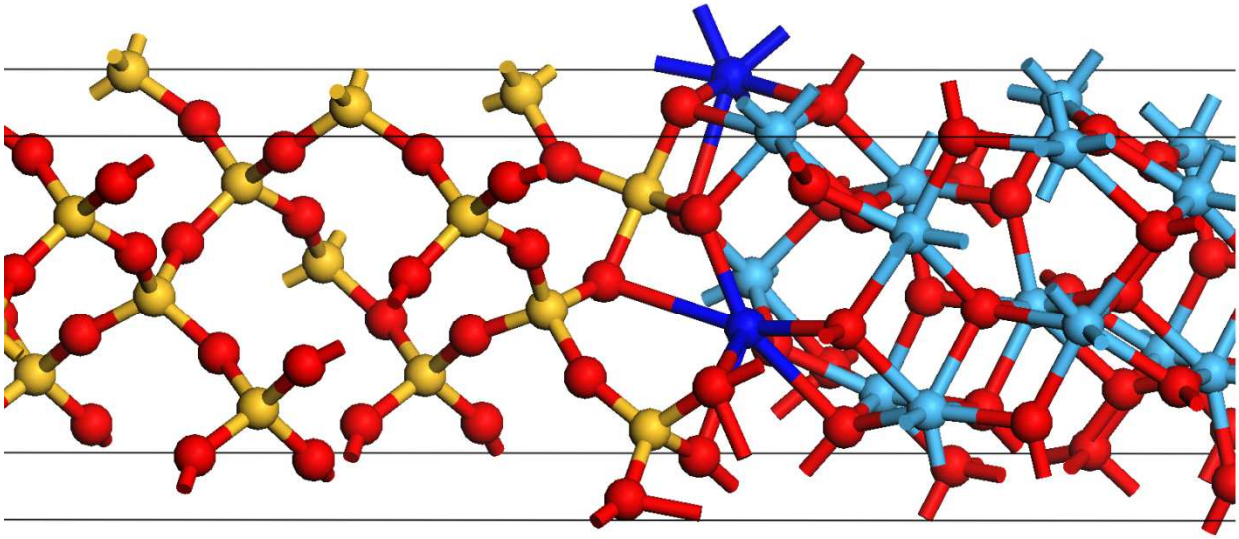

Figure 3d BF11791 27SEP2011

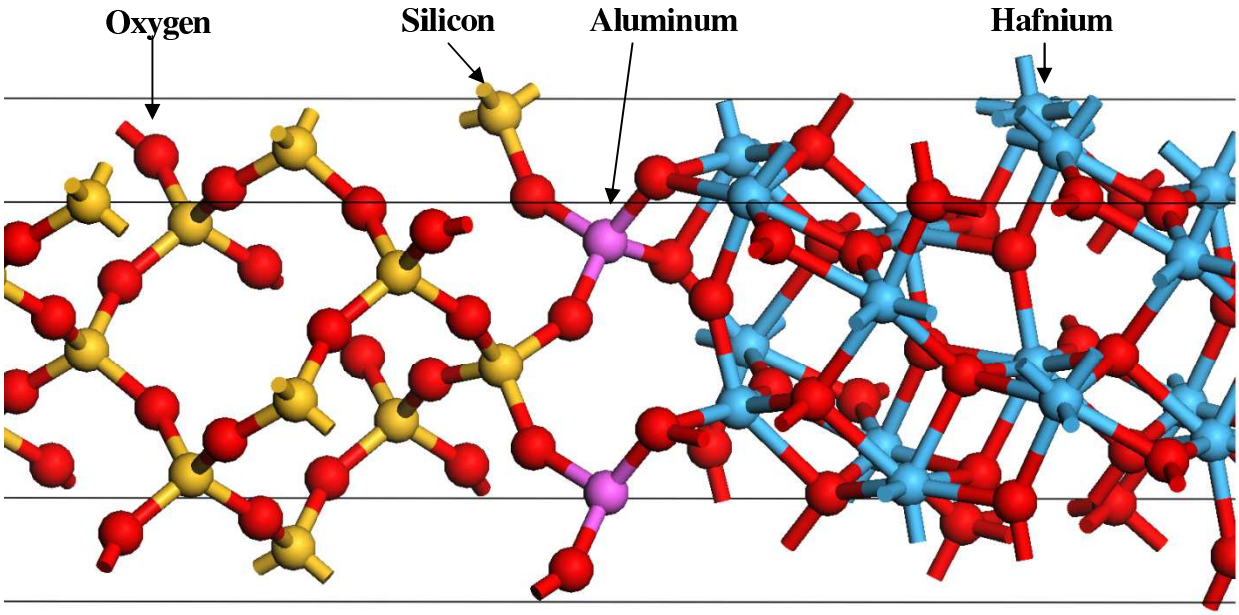

Figure 4a BF11791 27SEP2011

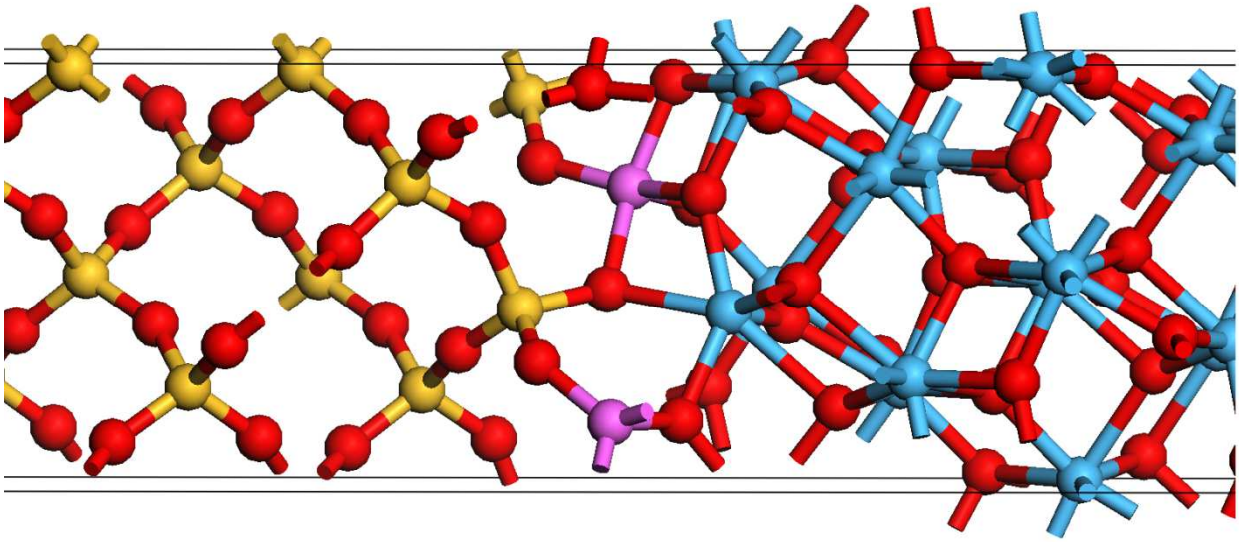

Figure 4b BF11791 27SEP2011

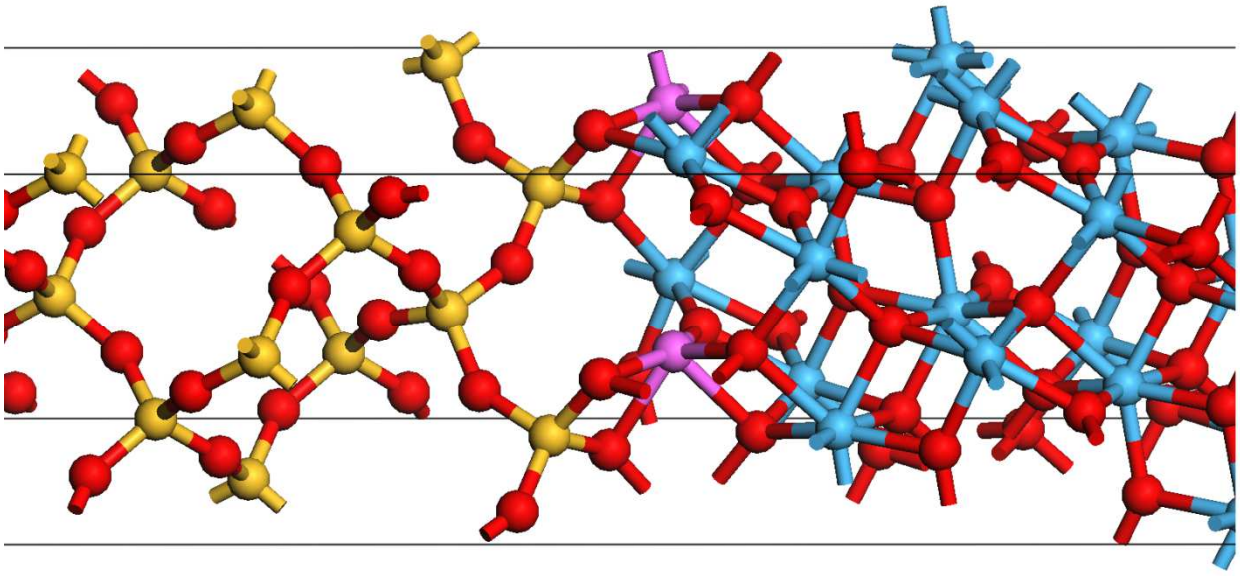

Figure 4c BF11791 27SEP2011

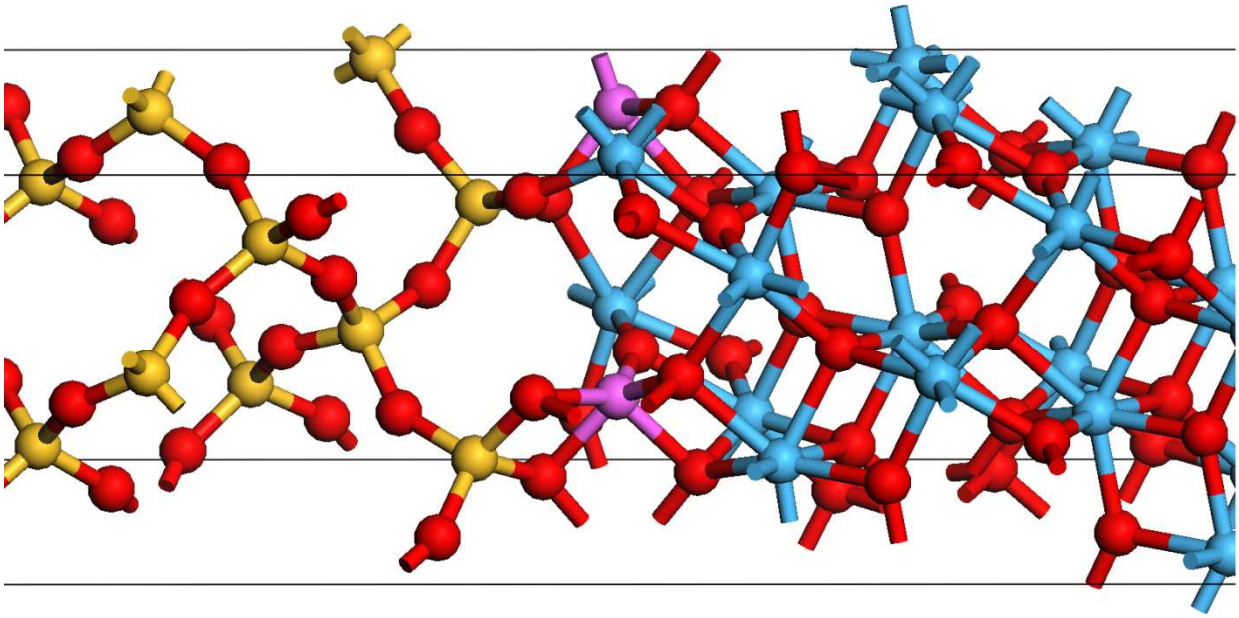

Figure 4d BF11791 27SEP2011

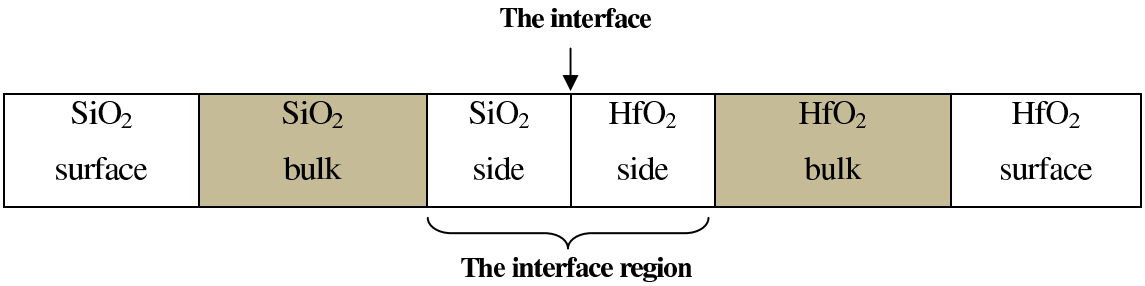

Figure 5a BF11791 27SEP2011

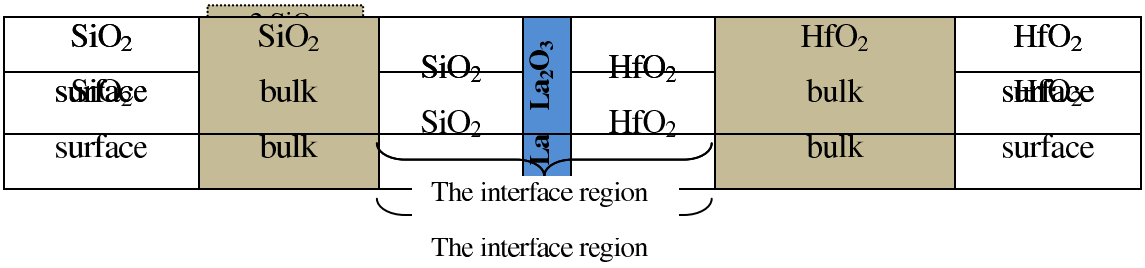

Figure 5b BF11791 27SEP2011

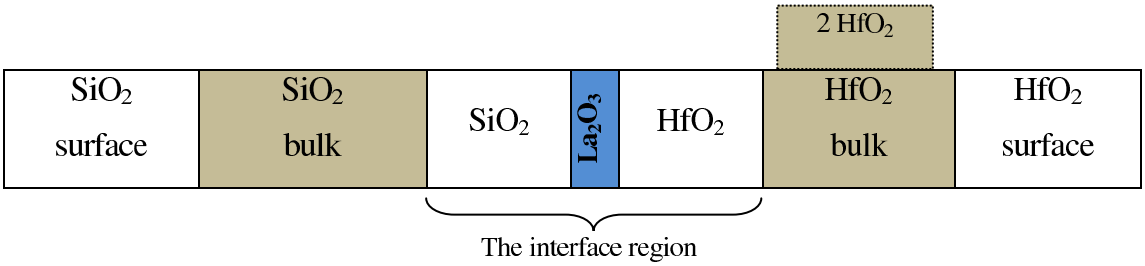

Figure 5c BF11791 27SEP2011

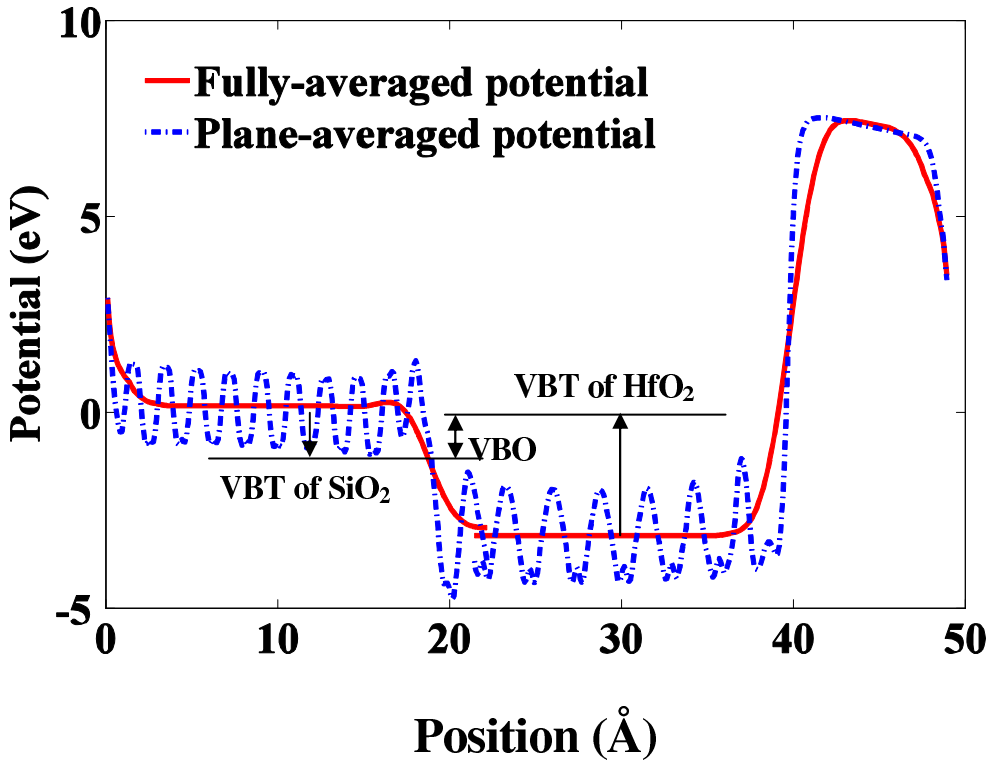

Figure 6 BF11791 27SEP2011

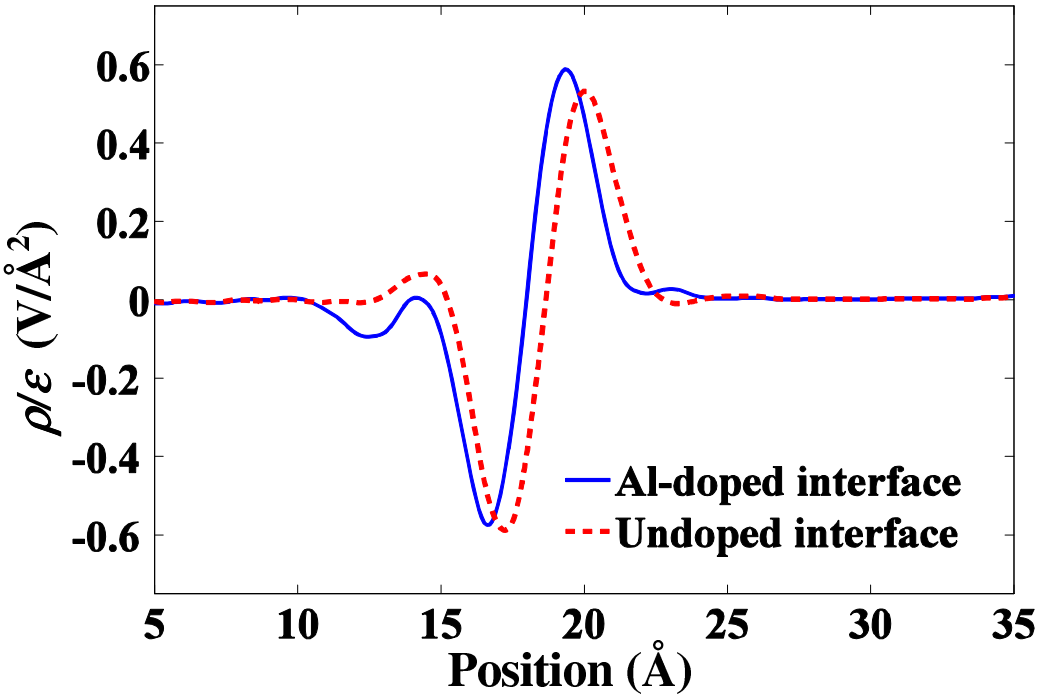

Figure 7a BF11791 27SEP2011

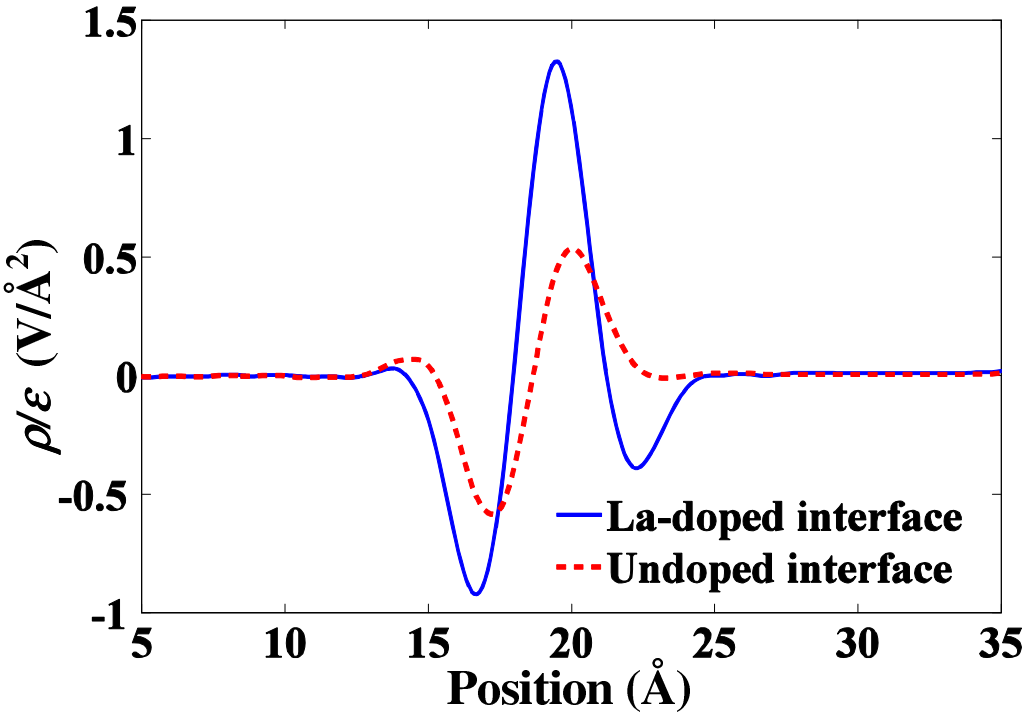

Figure 7b BF11791 27SEP2011

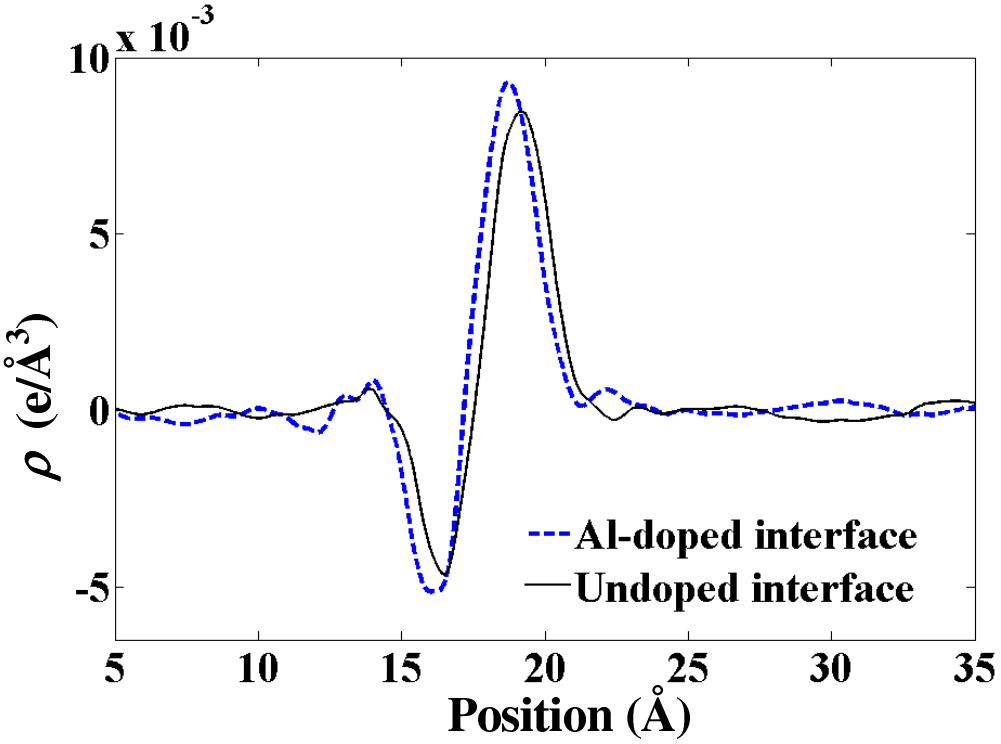

Figure 8a BF11791 27SEP2011

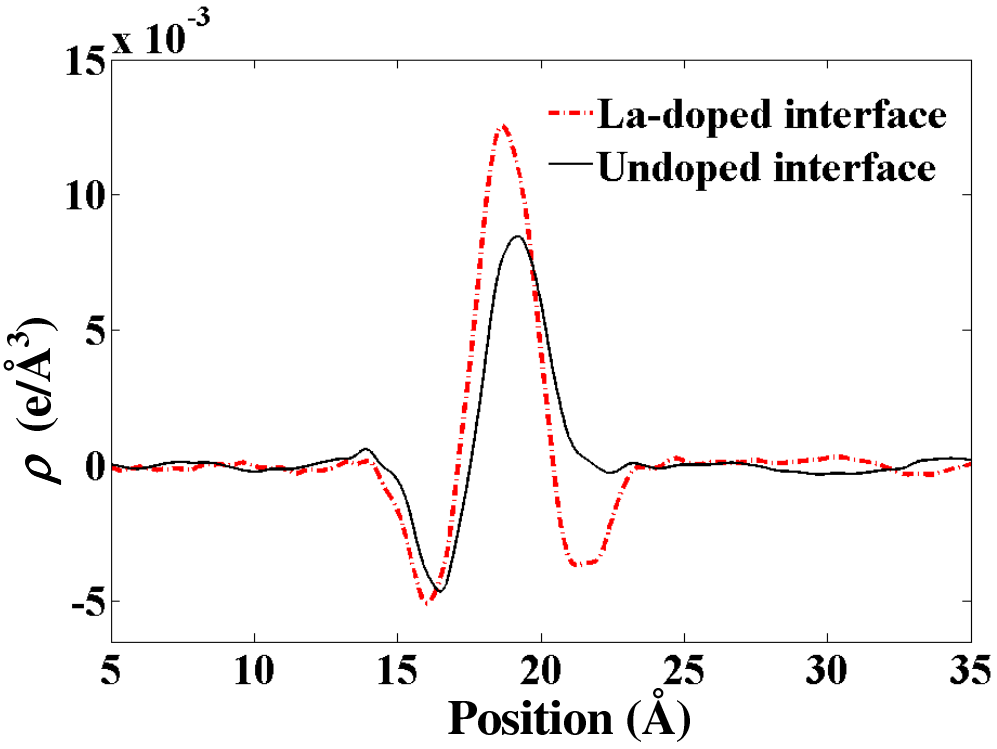

Figure 8b BF11791 27SEP2011

Figure 9a

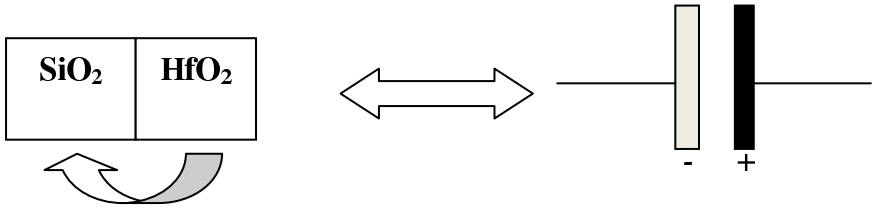

Figure 9b

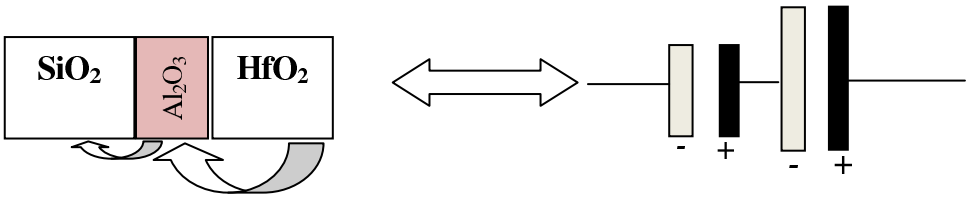

Figure 9c